

An Investigation into Length Scale Dominance in Critical Black Hole Formation

Cole Kelson-Packer* and John Belz†

*Department of Physics and Astronomy, University of Utah
Salt Lake City, UT 84112, U.S.A.*

(Dated: May 20, 2022)

The critical formation of low-mass black holes is a historical cornerstone of numerical General Relativity, with important implications in cosmology for censorship conjectures and the production of primordial black holes (PBHs). Concurrent with the surge in black hole observational physics in recent years has been an increased interest in these subjects. Critical formation is often suggested as a mechanism for PBH production, but it is possible that the existence of different types of critical formation potentially accompanying more realistic scenarios may affect this conclusion more than has been investigated thus far. This paper numerically investigates, as a toy model, the interplay of multiple near-critical fields in the critical collapse of spherically symmetric scalar fields. It is found that a combination of type I and type II near-critical fields results in a kind of competition between their respective critical evolutions and propose. A heuristic explanation for this phenomenon is given employing ideas from the theory of dynamical systems.

I. INTRODUCTION

Critical phenomena in black hole formation is one of the classic numerical results of General Relativity in the strongly interacting regime, dating back to Choptuik's [1] seminal paper on self-gravitating massless scalar fields. Similar critical phenomena without a mass gap have been discovered for a variety of different matter configurations, such as axially symmetric gravitational waves [2] and Yang-Mills fields [3]. Critical phenomena with a mass gap has also been discovered, for example in the study of massive scalar fields [4], and other "hair", such as charge and angular momentum, exhibit critical behavior as well [5–8]. A larger collection of results may be found gathered in a review by Gundlach [9]. Generally speaking, critical phenomena is a fine way of illustrating the richness of behavior accompanying the non-linear nature of Einstein's equations.

Most studies of black hole critical phenomena, with recent exceptions [10, 11], have considered a single type of constituent matter, and focus on initial data of that specific type belonging to various single-parameter families. This works well enough for illustrating criticality and quasi-universality, as the mass (or whatever quantity is of interest) depends on a difference of the parameter, while universality is suggested by the similarity of behavior for a variety of parameterized initial data. Conclusions from such investigations have been considered sufficient for most applications of the theory: cosmic censorship conjectures are adequately probed by what are essentially toy models [12, 13], whereas mechanisms for producing primordial black holes are modeled upon the density fluctuations of dominating matter sources [14].

What has been given less consideration is the implications that more realistic mixed matter configurations

could have for criticality. Loosely speaking, critical phenomena in general relativity are the manifestation of the existence of different basins of attraction in the phase space of solutions to Einstein's equations, all associated with critical solutions of varying co-dimension [15]. Different types of criticality, however, may be affiliated with different critical solutions: the evolution of massless scalar fields is influenced by the existence a self-similar spacetime [16, 17], whereas massive scalar fields exhibiting a critical mass gap are associated with metastable soliton stars [4]. From previous numerical studies [4] there would seem to exist interactions between the effects of different critical spacetimes: for critical massive scalar fields, a mass gap emerges and criticality shifts from type II to type I when the characteristic length scale of the initial field becomes sufficiently large. It is conceivable that the time evolution of more general composite configurations may be significantly affected by several critical solutions.

We test this idea in this paper. Considering spherically symmetric matter configurations that feature both a massless and a massive scalar field, we show using a two-parameter sample of initial conditions not only that three different phases of evolution behavior (corresponding to two collapse timescales and asymptotic dispersal) are displayed for this multi-field content, but that competition between the influence of the critical solutions associated to the two individual fields affects the critical evolution of these spacetimes. Our results are similar in nature to a recent, earlier work by Gundlach, Baumgarte, and Hilditch [10], resembling an alternative scenario they advance. An intriguing particularity highlighted by our results concerning the inhibiting effect of multi-critical configurations, however, suggests that a more nuanced approach may be necessary when considering the application of critical phenomena to more realistic scenarios.

* u0980902@utah.edu

† belz@physics.utah.edu

II. METHODS

Throughout we use Einstein summation convention and set c and $8\pi G$ to unity for convenience.

We employ the polar-areal gauge for our metric. The toy model we use for illustrating our conceptual idea consists of a pair of spherically symmetric scalar fields minimally coupled to gravity. One field is massless, exhibiting type II critical collapse when taken alone, as in Choptuik's original paper [1]. The other field is massive, with the mass, characteristic length scale, and initial conditions taken such that type I critical collapse would be exhibited if it were evolved on its own [4].

A. Matter Evolution

At the most general level, the Lagrangian for a collection of minimally coupled scalar fields is

$$L = \frac{1}{2} \nabla_\mu \Phi_i \nabla^\mu \Phi_i - V(\Phi_i). \quad (1)$$

With two fields, one massless, the other massive, and no other potential,

$$L = \frac{1}{2} \nabla_\mu \Phi_1 \nabla^\mu \Phi_1 + \frac{1}{2} \nabla_\mu \Phi_2 \nabla^\mu \Phi_2 - \frac{1}{2} m_1^2 \Phi_1^2. \quad (2)$$

A quick application of Euler-Lagrange yields the naive equations of motion:

$$\begin{aligned} \nabla_\mu \nabla^\mu \Phi_1 + m_1^2 \Phi_1 &= 0, \\ \nabla_\mu \nabla^\mu \Phi_2 &= 0. \end{aligned} \quad (3)$$

With our choice of metric,

$$g_{\mu\nu} = \text{diag}(-\alpha^2, a^2, r^2, r^2 \sin^2(\theta)), \quad (4)$$

the Laplacian may be readily expanded:

$$\nabla_\mu \nabla^\mu \Phi_j = \frac{1}{\alpha a} \partial_t \left(\frac{a}{\alpha} \partial_t \Phi_j \right) - \frac{1}{\alpha a r^2} \partial_r \left(\frac{\alpha r^2}{a} \partial_r \Phi_j \right). \quad (5)$$

Defining the following auxiliary quantities,

$$\Pi_i \equiv \frac{a}{\alpha} \partial_t \Phi_i, \quad \Psi_i \equiv \partial_r \Phi_i, \quad (6)$$

the equations (3) split into three pairs:

$$\begin{aligned} \partial_t \Phi_i &= \frac{\alpha}{a} \Pi_i & i = 1, 2, \\ \partial_t \Psi_i &= \partial_r \left(\frac{\alpha}{a} \Pi_i \right) & i = 1, 2, \\ \partial_t \Pi_i &= \frac{1}{r^2} \partial_r \left(\frac{\alpha r^2}{a} \Psi_i \right) - \alpha a m_i^2 \Phi_i & i = 1, 2, \\ & & m_2 = 0. \end{aligned} \quad (7)$$

On the numerical level, the usual accommodations (see e.g. [18]) are made for the third equation above so as to facilitate better behavior at the origin:

$$\begin{aligned} \partial_t \Pi_i &= 3 \frac{\partial}{\partial r^3} \left(\frac{\alpha r^2}{a} \Psi_i \right) - \alpha a m_i^2 \Phi_i & i = 1, 2, \\ & & m_2 = 0. \end{aligned} \quad (8)$$

Simple radiating boundary conditions are taken for the Π_i s, enabling the evolution of the Φ_i s and Ψ_i s using the same equations as above at the large-radius edge. This is sufficient, but imperfect; for large t , apparent convergence may eventually degrade even for dispersing initial conditions.

B. Metric Evolution

In the polar areal gauge the surface area of a sphere is held constant. This implies that the coefficient of the spherical area element $d\Omega$ is unity and that all components of intrinsic curvature K_{ij} are zero except for the radial-radial component [18]. With the shift β also chosen to be trivial, the ADM evolution equations simplify greatly. These choices mean that the only dynamical components of the metric are the lapse α and the radial-radial component a , which can be shown to satisfy the following equations:

$$\partial_r a = \frac{a}{2} \left[\frac{1-a^2}{r} + \frac{r}{2} \sum_{i=1}^2 (\Pi_i^2 + \Psi_i^2 + m_i^2 a^2 \Phi_i^2) \right], \quad (9)$$

$$\partial_r \alpha = \alpha \left[\frac{\partial_r a}{a} + \frac{a^2 - 1}{r} - \frac{m_1^2 r}{2} a^2 \Phi_1^2 \right]. \quad (10)$$

The first equation above arises from our demands upon the intrinsic curvature, while the second ultimately derives from the Hamiltonian constraint. The momentum constraint, meanwhile, yields the expression

$$0 = M \equiv \alpha \frac{r}{2} (\Pi_1 \Psi_1 + \Pi_2 \Psi_2) - \partial_t a, \quad (11)$$

whose numerical deviation from exact satisfaction we use to monitor convergence.

C. Numerical Technique

The basic underlying techniques we employ are standard, and may be found in most textbooks on numerical relativity, e.g. [18]. Starting from an initial configuration for the scalar fields belonging to a two-parameter space, we integrate equations (9) and (10) above using fourth-order Runge-Kutta to obtain α and a , demanding that $a = 1$ at the origin and $\alpha = 1/a$ at the boundary. Having obtained these metric components, we evolve the field components in time (also with fourth-order Runge-Kutta), allowing us to reintegrate a and α at the next time step and repeat. Sixth-order dissipation is employed [19], without which spurious oscillations with significant effects develop coincident with the apparent horizon.

Our numerical grid extends radially to $r = 400$. This limit was chosen for the reason that it is considerably larger than any (unit-equivalent) collapse time observed

at the parameter resolutions probed, without being ungainly. To give an idea, the longest time to collapse in the jobs shown in Fig. 8 is ≈ 150 . It is by the apparent failure to collapse, the decline in field amplitude, and the recovery of the lapse to ≈ 1.0 at such large times that we may safely conclude that particular spacetimes tend towards asymptotic flatness.

We use standard adaptive step size with Richardson extrapolation and multi-grid techniques [20] to greatly reduce computation time near criticality, without which a computationally prohibitive number of gridpoints would be required for accurate evolution.

III. RESULTS

A. Convergence

We first provide evidence of the expected fourth-order convergence, illustrated by the following figures. Taking a field configuration asymptotically dispersing with numerical boundary at $r = 300$, we plot in Fig. 1 the behavior of the apparent order of convergence as measured by momentum constraint violation. The results of the same setup, except with the numerical boundary stretched to $r = 400$, is plotted in Fig. 2. In this second graph, we see that the apparent order of convergence does not begin oscillating until later. Finally, convergence for setup with initial conditions such that collapse occurs (with numerical boundary at the much smaller limit of $r = 40$) is shown in Fig. 3. The early decline in order in this last case may be attributed to two causes: the simultaneously numerically and physically significant fact that the polar areal gauge is not able to effectively evolve spacetimes for long after black hole formation, and the purely numerical fact that the differential equations for the metric become increasingly stiff as the lapse collapses. In all graphs the ordinate value is a measure of the apparent order observed, which should be ≈ 4 or 5 (courtesy of Richardson extrapolation and multigrids) if the scheme is converging. This order is obtained via

$$\text{error ratio} = \ln \left(\frac{\text{rms}(M_{4000})}{\text{rms}(M_{8000})} \right) / \ln(2). \quad (12)$$

Altogether, these figures suggest that the numerical algorithm used exhibits convergence, and hence the results obtained are not numerical artifacts.

B. Scale Interaction

The presence of two near-critical fields associated with different critical spacetimes results in competition between their respective evolution tendencies. We consider individually, as a specific example, a massless field configured to disperse and a massive field configured to collapse, both with Gaussian-like initial data. We plot the

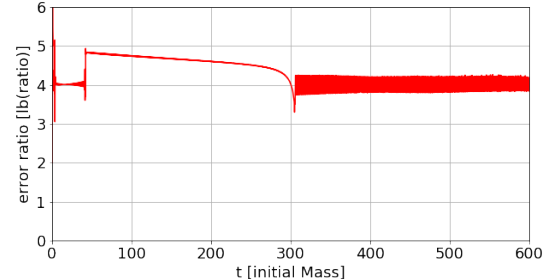


FIG. 1: Approximate order of convergence given as a ratio of rms momentum constraint violation for 4000 and 8000 coarse gridpoints over time for disperse scenario. Initial conditions are somewhat close to criticality. Numerical boundary is at $r=300$. The jump in convergence order at $t \approx 40$ is a consequence of a secondary grid activating.

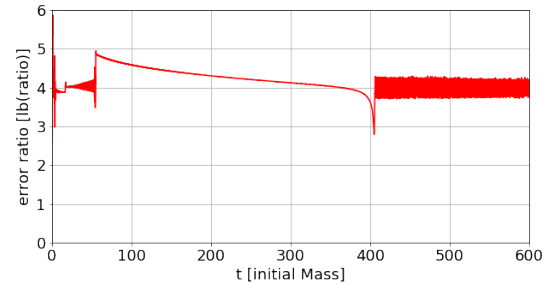


FIG. 2: Approximate order of convergence given as a ratio of rms momentum constraint violation for 4000 and 8000 coarse gridpoints over time for disperse scenario. Initial conditions are somewhat close to criticality. Numerical boundary is at $r=400$. The jump in convergence order at $t \approx 60$ is a consequence of a secondary grid activating.

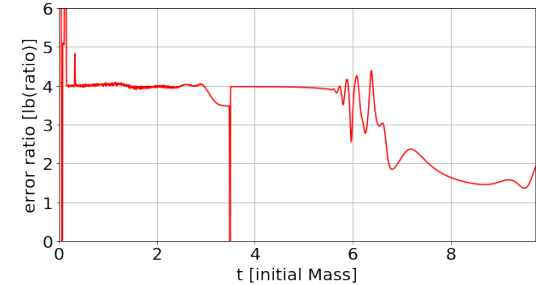


FIG. 3: Approximate order of convergence given as a ratio of rms momentum constraint violation for 4000 and 8000 coarse gridpoints over time for collapse scenario. Numerical boundary is at $r \approx 40$. The apparent dip at $t \approx 3$ is due to a secondary grid appearing surrounding the origin. The black hole begins to form around $t \approx 6$. Initial conditions are somewhat close to criticality.

resulting behavior for the fields and lapse at the origin in Fig. 4. Figure 5, meanwhile, shows the behavior for two fields minimally coupled. The apparent space-filling in many of these graphs, both for the fields and the lapse, is not numerical error, but rather the result of rapid os-

ciations: this is shown by the inset in the first image of Fig. 5. This is an expected consequence of the extra time-scale introduced by the mass – the massless case notably does not feature such rapid variation.

It is notable that *no* collapse occurs in Fig. 5, despite the initial data having greater mass-energy content than either near-critical constituting field taken alone. This surprising result suggests that the two fields frustrate, rather than enhance, their respective critical evolutions. In this strongly-coupled system we are seeing nonlinear phenomena overruling common intuition.

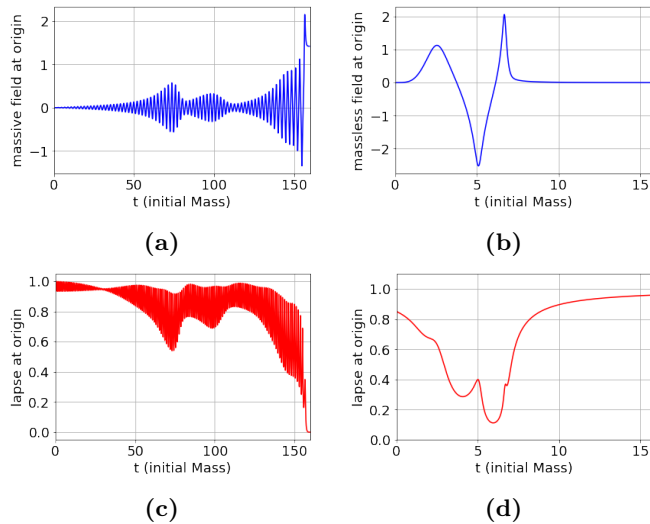


FIG. 4: Graphs of Φ (top) and α (bottom) at the origin for Type I and type II critical fields. The massive field, in the left column, is supercritical, while the massless field on the right is subcritical.

Nor is this oddity dependent upon any quirk of the initial data, as should be expected given the underlying quasi-universality. Taking the massless field to be a shifted hyperbolic tangent function as its initial data yields similar results. Figure 6 illustrates the the behavior of each field alone, while Fig. 7 shows the evolution of the two taken at once.

We have obtained, as shown in Fig. 8, a kind of phase diagram for the asymptotic behavior of our composite critical configuration. Each individual point represents an independent simulation, with the the abscissa and ordinate values specifying the amplitudes for the massive and massless initial fields respectively. The marker shapes classify the spacetimes by apparent end behavior, distinguishing dispersal (circles), type I collapse (triangles), and type II collapse (diamonds). The method utilized for this classification is crude, but sufficient: collapses occurring < 40 time units are classified as type II, collapses occurring thereafter up to $t = 400$ time units are classified as type I, and spacetimes showing no signs of collapse up to $t = 400$ are deemed asymptotically dispersing. This cutoff time is well more than necessary, since the greatest collapse times occur at ≈ 160 time

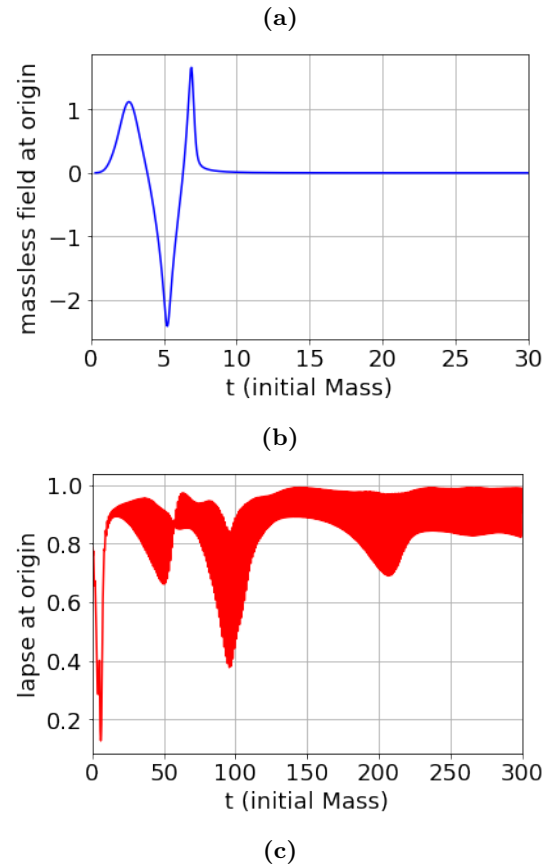
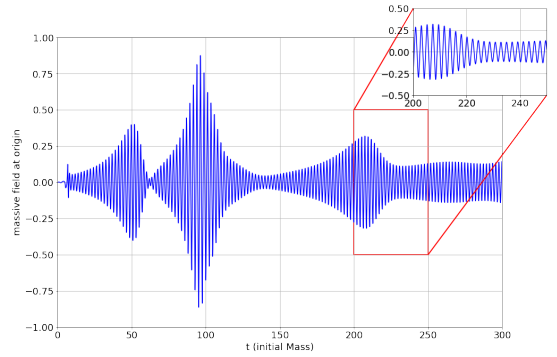


FIG. 5: Graphs of the Φ s and α at the origin for mixed field content. The inset for (a), depicting the massive field, illustrates how rapidly the field varies. No collapse occurs despite the initial field content being a combination of the two fields whose time evolutions are depicted individually in Fig. 4 *supra*.

units at the parameter resolution probed. Meanwhile, the color scale applied to the points reflects the black-hole mass at the time of collapse, set to dark red (zero mass) for dispersing spacetimes. Three distinct domains emerge in both classification schemes, which are found to be in complete agreement with each other.

The solid black horizontal and vertical lines in the same figure denote the approximate critical parameter for two fields if they were taken alone. Figure 8 shows, however,

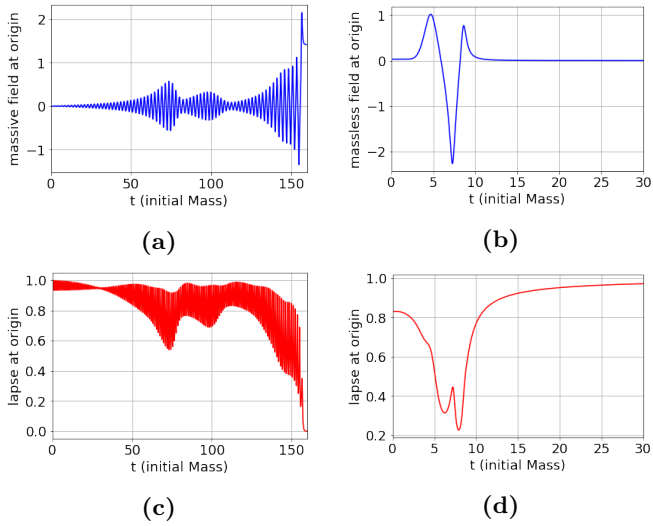


FIG. 6: Φ (top) and α (bottom) at the origin with hyperbolic tangent initial data for the massless field. The massive field, in the left column, is supercritical, while the massless field on the right is subcritical.

that the three domains are not circumscribed by these lines as might be predicted by intuition. The asymptotically dispersing domain is raised slightly into the would-be type II critical region, and also bent rather noticeably into what might naively be taken to be the type I supercritical region. Our specific scenario hence shows that multicritical configurations can actually have an *inhibiting* influence on black hole formation.

IV. DISCUSSION

In a sense, there are in fact only really two domains if the configurations are looked at in the asymptotic time limit: either a single black hole forms, or the fields disperse and spacetime tends towards flatness asymptotically. The spacetimes exhibiting gravitational collapse at smaller timescales would feature growing black holes as time progressed (courtesy of the second still-ingoing field), which would be seen if more delicate evolution techniques were employed (also greatly increasing the computational cost). Nevertheless, the apparent existence of vastly differing timescales to collapse, in conjunction with the growth of the asymptotically dispersing region and the sharp changes in behavior in the configuration space, suggest that different dynamics are responsible for controlling the evolution of spacetimes in each of these three domains – in other words, which modes dominate. The boundaries between apparent regions shown above, hence, are indicative of the structure of the relevant system of attractors at play in our scenario.

We suggest a simple dynamical systems picture for understanding this effect. As is well known [15] for a single field, critical collapse is the consequence of the existence

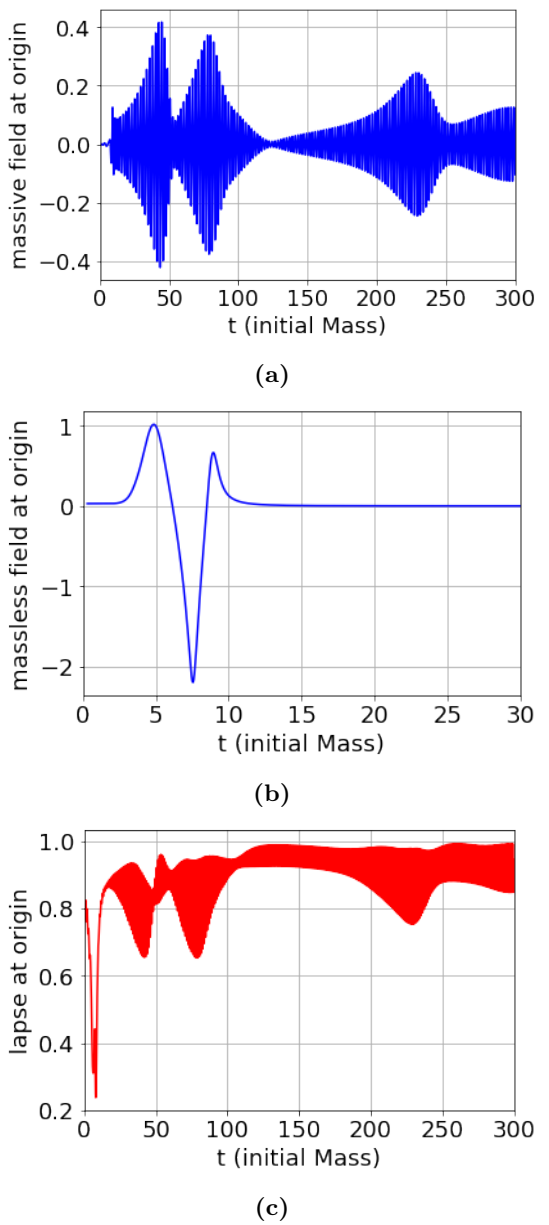


FIG. 7: Graphs of Φ and α at the origin with hyperbolic tangent initial data for the massless field. No collapse occurs despite the initial field content being a combination of the two field evolutions depicted individually in Fig. 6 supra.

of an attractor of some codimension in the phase space of solutions to Einstein's equations. Initial data belonging to a one-parameter curve of initial data will intersect the surface of attraction at a single point corresponding to the critical value. Initial data given by configurations with parameter slightly greater or less than criticality will, after (a possibly lengthy) critical evolution, be repelled in opposite "directions" from the surface of attraction towards different asymptotic limits – black hole formation, or dispersal to flat space.

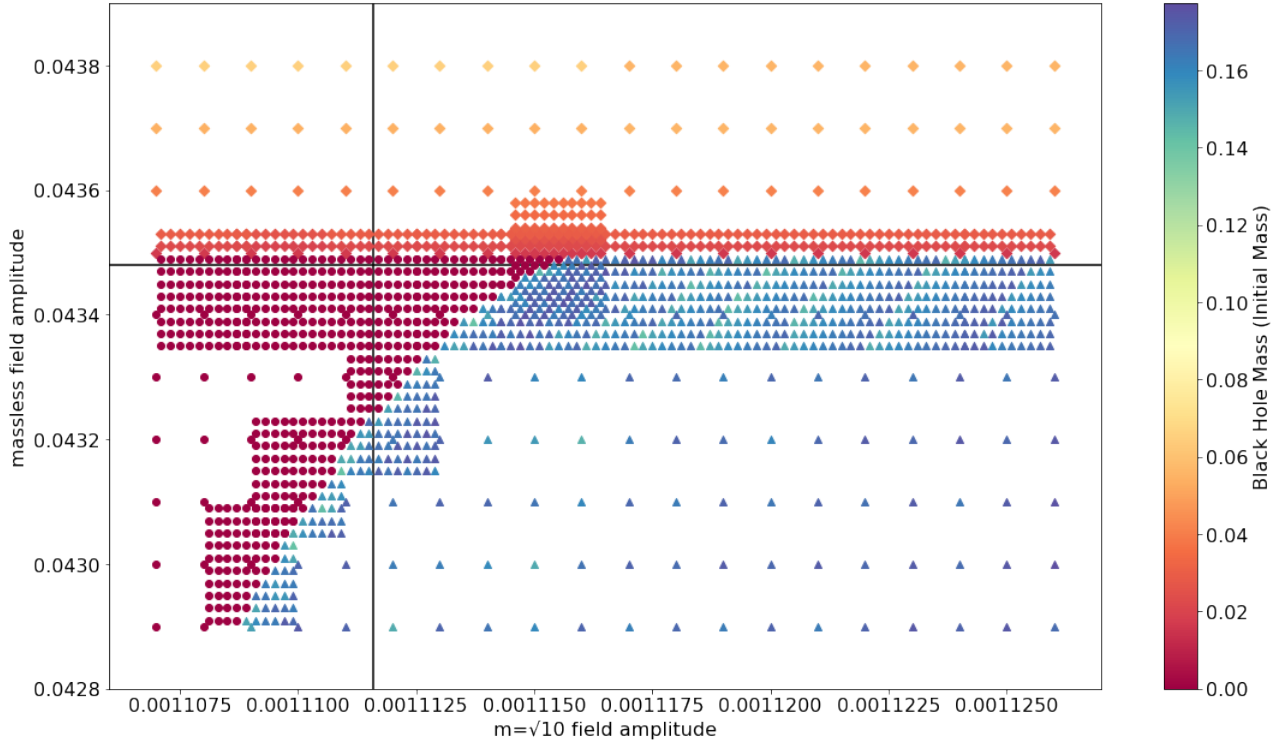


FIG. 8: Phase diagram of time evolution behavior for the multi-critical field configuration considered in this paper. The axis variables correspond to the parameters tuning the initial data for the scalar fields that ultimately determine whether collapse or dispersal occurs. The circles indicate dispersal, the triangles denote type I collapse, and the diamonds are type II – this is determined by collapse times (or the lack thereof). The color scale is a measure of the mass of the black hole formed. If the initial data evolves to be asymptotically dispersing, this is set to zero mass with a dark red. The approximate critical quantities for the individual fields are 0.04347 and 0.0011116. The above picture suggests that the competition between the two associated critical spacetimes considered here has an inhibiting effect on criticality.

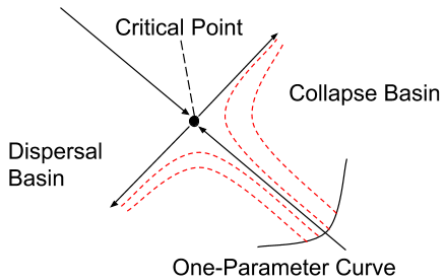


FIG. 9: Simplified picture of the nature of critical phenomena for a single field. The dashed trajectories denote the time evolution of spacetimes with initial conditions on the parametrized curve. The arrows suggest the direction of the locally dominant time evolution mode: a single attracting surface, here represented as a point, is attractive (has arrows pointing to it) on a submanifold of some codimension. In directions normal to this submanifold it is repulsive (has arrows pointing away from it), so a one-parameter line of initial data not lying exactly in this submanifold may have points close to intersection with vastly differing asymptotic behaviors.

However, when two or more near-critical fields are in

play at once, and the two fields are configured individually to have their evolutions determined by two different critical surfaces, then a more complex picture could emerge in which the two attracting surfaces are in a sense in competition. As a consequence, the stronger attractors (heuristically corresponding to the critical surface with larger inverse time-scale, corresponding to the smaller mass solution – the massless type II critical solution in our case) will “pull” initial data away from other attractors, possibly resulting in dispersal to flat space for some configurations despite being supercritical with respect to one of the parameters. This effect is observed in our phase space picture in Fig. 8 cohabitant with significant curvature of the domain separation, which supports this interpretation. What is surprising here is the dispersal of spacetimes whose initial conditions are such that a black hole would otherwise form but for the presence of the competing field.

Our results should be compared with a recent, earlier paper by Gundlach, Baumgarte, and Hilditch [10]. In their paper, they consider the interaction of an SU(2) Yang-Mills field with a massless scalar field, with the intent of investigating what effects gravitational waves might have on critical collapse. They find that the scalar

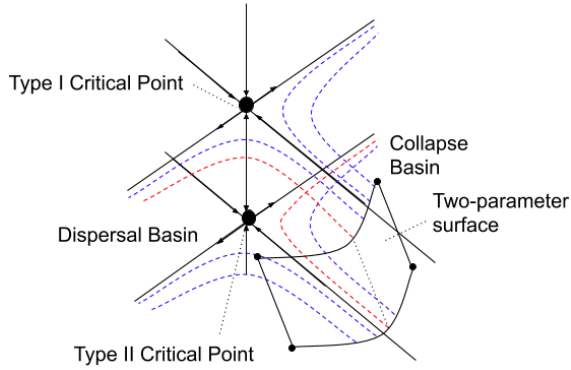


FIG. 10: Simplified picture of the possible dynamics for competitive critical phenomena. The dashed trajectories denote the time evolution of spacetimes with initial conditions on the parametrized surface, while the arrows suggest the direction of locally dominant time evolution modes. Because the influence of two different attractors is relevant, there is a kind of competition between their effects as initial data is “pulled” towards both surfaces, in a sense inhibiting the criticality of both. The pair of red dashed trajectories denote the time evolution of initial fields having equal massless field parameters, but different massive field parameters. This picture shows how attraction to a secondary critical point may, in a nontrivial way, inhibit a configuration’s tendency to collapse in spite of an increased mass-energy density.

field (acting as a toy model of gravitational waves) in fact dominates on smaller scales, and postulate the existence of a family of “quasi-discretely self-similar” spacetimes with one unstable mode that controls the evolution of their mixed field configuration. These postulated families interpolate between the critical spacetimes of the individual field constituents, moving from pure Yang-Mills in the distant past to pure scalar in the distant future.

Gundlach et al. explain this scenario from a quasi-dynamical systems perspective, with one of the Yang-Mills critical solution’s unstable modes directed towards the critical scalar solution, which has but a single unstable mode. This picture, illustrated in Fig. 12 of their paper, loosely resembles the scenario we conjecture in Fig. 10. However, they also briefly suggest the existence of an alternative scenario for other mixed field configurations (they give the example of two massless scalar fields) with *three* critical spacetimes: one for each of the two constituent fields, each with a single unstable mode, and a third with a pair directed towards the other critical solutions. Our case more closely exhibits this latter scenario, with the third hypothetical critical solution positioned along the frustrated axis containing the type I and type II critical points in Fig. 10. If this is so, then our conjectured scenario very much resembles Fig. 13 of their paper. Precisely this is suggested by Fig. 8. Each boundary is indicative of an unstable mode directed away from a particular attractor of some codimension. There appears to exist a kind of triple point, deviation from

which along two of the boundaries leads to what would appear to be the type I and type II critical solutions. Movement along the third boundary between the type I and type II regions, meanwhile, is in fact only movement towards the generic asymptotic black hole, as explained at the beginning of this section. This last boundary is hence symptomatic not of another family of critical solutions in addition to the triple point, but rather the different modes dominating time evolution.

It is interesting, nevertheless, how different the time scales of the “critical” evolution on either side are – we interpret this to be a consequence of the vastly differing criticality types investigated. It is possible that the alternate scenario briefly alluded to in Gundlach et al.’s paper containing two massless scalar fields might show a similarly exaggerated difference in time scale if, for example, both fields were taken to be initially thin shells, with one field localized at a significantly greater radius. Such a configuration, however, would likely not exhibit the same mass behavior at the time of collapse which so readily illustrates which modes dominate time evolution for a given initial datum. Moreover, it seems likely that a configuration with two massless scalar fields, or more generally two fields associated to the same type of criticality, would rather enhance criticality, decreasing the critical value along either axis of the two parameter space (assuming both parameters to be positively correlated with energy density). This, if true, would contrast with our results, which exhibits instead the inhibiting influence of multi-criticality.

V. CONCLUSION

We have found that the evolution of initial data containing multiple fields tuned near-criticality with respect to distinct critical surfaces exhibits a kind of competition between the critical surfaces. On a higher level, this is consistent with the results of a recent paper by Gundlach et al. [10], though we employ different methods and analyze a different scenario. This behavior is expected of the Einstein equations if they are approached with the philosophy of dynamical systems. Though this paper only made use of two scalar fields, it is likely that this phenomenon generalizes for the case of more fields and more varied matter content. Moreover, we have no reason not to expect other dynamical systems phenomena, such as bifurcation, to manifest in other regions of the parameter space of initial conditions away from multi-points. Outside the well-behaved region containing the triple point seen in Fig. 8, we have found more complex behavior near the boundary between type I collapse and dispersal – this is the subject of ongoing study.

This interaction may have implications for cosmology in the production of PBHs. The effect observed would seem to indicate that combined matter configurations may in fact at times inhibit critical formation, which necessitates a more delicate treatment of fluctuations when

applying critical black hole phenomena to PBHs.

ACKNOWLEDGMENTS

We thank Philip Beltracci, Benjamin Bromley, Eric Hirschmann and David Neilsen for valuable discussions,

and Tugdual LeBohec for the donation of processor time used in the calculations presented here. We also gratefully acknowledge the technical support of the Center for High Performance Computing at the University of Utah.

- [1] M.W. Choptuik, Phys. Rev. Lett. **70**, 9 (2005).
- [2] A.M. Abrahams and C.R. Evans, Phys. Rev. Lett. **70**, 2980 (1993).
- [3] M. W. Choptuik, T. Chmaj, and P. Bizon, Phys. Rev. Lett **77**, 424 (1996).
- [4] C.M. Chambers and S.M.C.V. Goncalves, Phys. Rev. D **56**, 6057 (1997), gr-qc/9709014.
- [5] C. Gundlach and J.M. Martin-Garcia, Phys. Rev. D **54**, 7353 (1996).
- [6] S. Hod and T. Piran, Phys. Rev. D **55**, 3485 (1997).
- [7] R. Petryk, Master's thesis, University of British Columbia (2006).
- [8] C. Gundlach, Phys. Rev. D **65** (2002), gr-qc/9906124.
- [9] C. Gundlach, Living Rev. Relativity **10** (2007), gr-qc/0711.4620.
- [10] C. Gundlach, T.W. Baumgarte, and D. Hilditch, Phys. Rev. D. **100**, 1, gr-qc/1908.05971.
- [11] B.Kain, Phys. Rev. D **99** (2019), gr-qc/1905.04355.
- [12] D. Christodoulou, Comm. Math. Phys. **93**, 171 (1984).
- [13] R.M. Wald, Tech. Rep. EFI 97-43 (APS, 1997) gr-qc/9710068.
- [14] J. C. Niemeyer and K. Jedamzik, Phys. Rev. Lett **80** (1998), astro-ph/9709072.
- [15] C. Gundlach, Phys.Rept **376**, 339 (2003), gr-qc/0210101.
- [16] C. Gundlach, Phys. Rev. D. **55**, 695 (1997), gr-qc/9604019.
- [17] C. Gundlach, Phys. Rev. Lett. **75**, 3214 (1995), gr-qc/9507054.
- [18] M. Alcubierre, *Introduction to 3+1 Numerical Relativity* (Oxford University Press, 2008).
- [19] B. Gustafsson, H.O. Kreiss, and J. Oliger, *Time dependent problems and difference methods* (John Wiley, 1995).
- [20] Press, Teukolsky, Vetterling, and Flannery, *Numerical Recipes: The Art of Scientific Computing* (Cambridge University Press, 2007).